Energy Conversion and Management 289 (2023) 117164

Contents lists available at ScienceDirect

Energy Conversion and Management

journal homepage: www.elsevier.com/locate/enconman

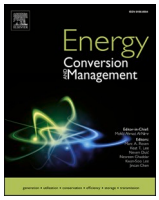

A molecular investigation on the mechanism of co-pyrolysis of ammonia and biodiesel surrogates

Zhihao Xing, Cheng Chen, Xi Jiang *

School of Engineering and Materials Science, Queen Mary University of London, Mile End Road, London E1 4NS, UK

ARTICLE INFO

Keywords:
Ammonia
Biodiesel
NO
Pyrolysis
Reactive molecular dynamics
Soot

ABSTRACT

As renewable energy sources with great potential to reduce carbon footprints and pollutant emissions, ammonia and biodiesel both have garnered substantial research interest. This study aimed to investigate the detailed mechanism of co-pyrolysis of ammonia and biodiesel surrogates, including the pyrolysis of different biodiesel surrogates, the effect of biodiesel decomposition on ammonia reactions, nitric oxide (NO) generation during the ammonia-biodiesel reaction process, and the effect of ammonia on soot formation during biodiesel pyrolysis. Using ReaxFF-based molecular dynamics simulations, the results revealed that the presence of ester groups in biodiesel lowers the activation energy of the reaction compared to alkanes. Meanwhile, biodiesel structures with shorter chain lengths, isomerisation, and carbon-carbon double bond effectively lower the activation energy. Time evolutions of the main pyrolysis products of methyl butanoate (MB), ethyl propionate (EP), and methyl crotonate (MC), as well as their detailed decomposition pathways, were produced. The coexistence of biodiesel and ammonia can promote the decomposition of ammonia, with MC containing carbon-carbon double bonds providing the most abundant free radical environment for ammonia decomposition. High temperature promotes the occurrence of the reaction, with MC, MB, and EP producing NO in the order of MC > MB > EP. Ammonia addition reduces soot production in the pyrolysis of different biodiesel surrogates, with MC exhibiting the most significant effect. The roles of oxygen-containing and nitrogen-containing species in soot suppression and their synergistic impact were identified at the atomic-scale. The insights into the detailed reaction mechanism of the co-pyrolysis of ammonia and biodiesel obtained in this study can be used to guide the development of ammonia-biodiesel co-firing technology.

1. Introduction

As a flexible long-term energy carrier and zero-carbon fuel, ammonia (NH_3) is attracting more and more research attention. In contrast to traditional fossil fuels, the combustion of ammonia can lower carbon emissions significantly [1]. Ammonia is widely available and can be produced from renewable sources. Some green ammonia pilot plants have successfully converted renewable energy sources (such as solar or wind power) into ammonia [2]. The use of green ammonia as a fuel will play a significant role in the decarbonisation of several industrial sectors such as marine transportation [3]. Ammonia has superior transport properties and lower storage costs than hydrogen (H_2), another zero-carbon energy carrier that has garnered substantial interest. Ammonia is not considered flammable during transportation, and its special odour allows ammonia leaks to be detected quickly [4]. Ammonia also has a high energy density. Since liquid ammonia has a volumetric density of around 1.5 times greater than liquid hydrogen, carrying ammonia requires a smaller infrastructure than transporting hydrogen [5].

Although ammonia combustion has a great potential in a wide range of applications such as heating, transportation and stationary power generation, there are various issues with using ammonia as a fuel that need to be resolved. Ammonia combustion generates nitrogen oxides (NO_X, including NO and NO_2) emissions [6,7], which seriously affects human health, causing damage to the alveolar structures and limiting their proper function [8]. Meanwhile, the low burning velocity, low heating value, and high auto-ignition temperature make the direct use of ammonia in combustion systems difficult [9]. One of the most plausible ways to improve the combustion of ammonia is to use a dual-fuel strategy [10], mixing ammonia with other highly reactive fuels, such as hydrogen, syngas (a mixture primarily consisting of hydrogen and carbon monoxide), dimethyl ether (DME), and hydrocarbons. The chemical kinetic mechanisms of ammonia combustion have been

* Corresponding author.
E-mail address: xi.jiang@qmul.ac.uk (X. Jiang).

https://doi.org/10.1016/j.enconman.2023.117164
Received 4 April 2023; Received in revised form 7 May 2023; Accepted 9 May 2023
Available online 25 May 2023

extensively studied, and it has been demonstrated that ammonia can mitigate the soot formation of hydrocarbon fuels [11]. Chen et al. [12] carried out experimental and chemical kinetic studies to analyse the laminar combustion characteristics of hydrogen/ammonia/air mixture. The results suggest that increasing hydrogen concentration in the fuel leads to an exponential increase in the laminar burning velocity (LBV) of the mixture. Additionally, increasing the amount of hydrogen promotes the generation of hydroxyl (·OH) and ·H radicals, which will accelerate the reaction. It was computationally shown that adding more hydrogen to ammonia intensified the reaction of ammonia/oxygen in the double-channel counter-flow micro-combustion system, but increased NO emissions [13]. A decrease in the mass fraction of hydrogen mixed with ammonia can lead to increased combustion instability [14]. The auto-ignition characteristics in ammonia-air and ammonia-hydrogen-air combustion were studied by applying direct numerical simulations under engine-relevant conditions [15]. It was found that pressure increase and hydrogen addition both can reduce the auto-ignition delay time. According to Chen and Jiang [16], the impact of hydrogen on the increase of LBV and net heat release rates in ammonia/air flame was the most significant, followed in decreasing order by syngas and CO. Cai and Zhao [17] found that adding DME increased the LBV of ammonia/air flames and altered the sensitivities of the main reactions, hence accelerating the overall reaction rate. Blending only 5% (by molar fraction) DME with ammonia can significantly reduce the ignition delay time of ammonia [18]. A reactive molecular dynamics simulation study conducted by Zhang et al. [19] revealed that methane (CH_4) promotes ammonia oxidation in the initial reaction stage, and this impact diminishes as the temperature increases.

One promising application of the dual-fuel strategy is the co-firing of ammonia with diesel, which remains an important fuel for heavy duty applications such as marine transportation although it is highly polluting. Diesel can be used as an additive for ammonia combustion, which increases the reactivity of ammonia and, at the same time, ammonia aids in resolving the carbon emission issues associated with diesel combustion [20]. Experiments have shown that the carbon-based emissions were reduced in ammonia-diesel dual fuel compression ignition (CI) engines with the increase of the ammonia energy share, while the emissions of NO, NO_2, and N_2O (a potent greenhouse gas) increased [21]. The primary concern for using diesel type of fuels is the harmful emissions of soot, also known as black carbon. Soot and its co-pollutants are the key components of fine particulate matter, i.e., $PM_{2.5}$, the leading environmental cause of cardiopulmonary mortality. Moreover, some studies have identified black carbon as the second largest anthropogenic contributor to global warming [22]. Some researchers have proven that ammonia can help reduce soot formation during diesel combustion. Cheng et al. [23] conducted an experimental and numerical study to analyse the effects of ammonia addition on soot formation in n-heptane laminar diffusion flames. They found that the addition of ammonia efficiently reduced soot formation by inhibiting the growth of polycyclic aromatic hydrocarbon (PAH). This is because the decrease of methyl ($\cdot CH_3$) radicals leads to a reduction of $\cdot C_4H_5$, a crucial precursor to forming the first aromatic ring. Their further research [24] observed that adding ammonia into n-heptane would make the structure of the produced soot looser and more chain-like, and this structure of soot is more likely to be oxidised. Ammonia-coal blending is also believed to be effective in reducing soot emissions during coal combustion. Experimental results show that both the number density and the size of soot particles decreased after co-firing ammonia with coal under fuel-rich conditions [25].

The urgent need of decarbonisation requires a rapid transition to lower-carbon energy sources. Biofuels produced from biomass are renewable alternatives to fossil fuels with the hope of achieving environmental and socioeconomic benefits such as reducing anthropogenic greenhouse gas (GHG) emissions, promoting rural development, generating employment and increasing energy security. Biodiesel, i.e., fatty acid methyl esters (FAMEs) and bioethanol, are currently two of the commercially available large-scale biofuels that can be produced from various resources [26–28]. Most of the blended fuel made by mixing biodiesel, bioethanol, and diesel is economically and environmentally superior to pure diesel fuel, and also improves the exergetic indicators of the system [29]. The properties of FAMEs are similar to fossil diesel, accordingly it can be employed in existing diesel engine infrastructure without major modifications to the engine [30]. The utilisation of biodiesel in conventional internal combustion engines resulted in particulate emission reduction appreciably under operating conditions owing to the oxygenated moiety within the primary fuel molecules, which changes the reaction rates and pathways of ignition and oxidation processes. Soot reduction is directly related to the added oxygen content, but not all oxygenated additives are equally effective. An in-depth understanding of the topic has not been achieved. Evaluating and quantifying the effects of actual biodiesel molecular structures, e.g., chain length, unsaturation degree and oxygenated moiety on sooting tendency, are currently lacking but essentially needed for the design of novel oxygenated biofuel additives. Compared to diesel, biodiesel contains oxygen which leads to more complete combustion and should be more favourable for promoting ammonia decomposition. Moreover, biodiesel has a higher Cetane number than diesel [31], which means the fuel ignites more easily and completely, leading to improved combustion. Although changes in key products, such as soot particles, CO, and NO during the co-firing of ammonia and biodiesel, have been noticed, there is a lack of in-depth understanding on the mechanisms involved. Sivasubramanian et al. [32] found that blending 20% ammonia with mustard biodiesel efficiently reduced hydrocarbon, CO, and smoke emissions. Nadimi et al. [33] analysed the emissions from an ammonia/biodiesel dual-fuel CI engine. They came to the same conclusion as Sivasubramanian et al. [32] and found that the NO emission increased as more ammonia was added. Ronan et al. [34] compared two combustion mechanisms for ethanol/ammonia blends and found that neither can adequately match the experimental data, indicating that more in-depth studies are needed to provide highly accurate kinetics mechanisms for such mixtures. Cardoso et al. [35] found that co-firing biomass and ammonia with coal can reduce NO and carbon emissions from coal combustion. They also indicated that further research is needed to investigate the detailed chemical kinetics concerning the interactions between coal, biomass, and ammonia.

The reactive force field (ReaxFF) based molecular dynamics (MD) method is widely applied in studying fuel pyrolysis, combustion and the soot formation process from a molecular point of view [36]. Wang et al. [37] analysed the reaction mechanism of methane/ammonia combustion using ReaxFF. Their results show that methane promotes the combustion of ammonia. Zhang et al. [38] combined experimental and ReaxFF studies to analyse the effects of ammonia addition on soot suppression during ethylene-ammonia co-firing. They concluded that the formation of nitrogen-carbon molecules reduces the number of molecules with small carbon numbers (below C_4 species), which are precursors of PAHs. The produced nitrogen-carbon species, such as cyanide (CN) radicals and HCN, would occupy the active sites on PAHs to suppress their further growth. The study showed that ReaxFF is feasible in studying the chemical effects of highly reactive fuels on ammonia and the inhibitory effect of ammonia on soot formation.

It is important to understand the detailed mechanism by which ammonia inhibits biodiesel carbon soot production and how biodiesel affects the reactions of ammonia, where a fundamental understanding is not yet available. This motivated the current study, which used reactive MD simulations to evaluate the co-pyrolysis of biodiesel surrogates and ammonia at the atomic-scale. Detailed reaction pathways and pyrolysis kinetics of biodiesel surrogates were analysed first, providing a basis for understanding their interactions with ammonia. The co-pyrolysis mechanism was analysed from three aspects: the impact of biodiesel pyrolysis on ammonia reactions, NO (the main NO_X species observed in ammonia-biodiesel co-pyrolysis reactions) generation, and how ammonia decomposition reduces soot production.

2. Methodology

2.1. Construction of the fuel model

Practical biodiesels are mixtures of FAMEs with various compositions. For example, rapeseed methyl esters are composed of esters ranging from C_{14} to C_{22}, some of which contain carbon-carbon double bonds in their molecular structure [39]. The ester group is related to soot mitigation or suppression of biodiesel (in comparison to fossil diesel) in fuel pyrolysis and combustion. Due to the complexity of the fuel mixture, it is difficult to identify the effects of all the molecular functions. Therefore, a practical solution is to use a simple and well-characterised surrogate model. In this study, methyl butanoate (MB, $C_5H_{10}O_2$), which is a simple C_5 ester, was considered in the simulations as it is believed to reflect the impact of oxygen atoms in biodiesel molecules [40]. The ethyl propionate (EP, $C_5H_{10}O_2$) and methyl crotonate (MC, $C_5H_8O_2$) were also simulated to compare with MB to interpret the effect of the isomerisation and the degree of unsaturation of biodiesel molecular structure on soot suppression. The methyl decanoate (MDN, $C_{11}H_{10}O_2$) is compared with MB to evaluate the impact of the carbon chain length of biodiesel surrogates. The pyrolysis of the n-alkane, i.e., n-dodecane (DDC, $C_{12}H_{26}$), is also calculated to highlight the effects of the ester group by comparing it with the pyrolysis of MDN. The molecular structures and chemical formulas of biodiesel surrogates, n-dodecane, and ammonia are shown in Fig. 1.

The detailed system constructions are shown in Table 1. Systems 1 to 3 are built as a baseline with pure biodiesel surrogate molecules and argon (Ar) molecules. Systems 4 to 6 and 7 to 9 represent biodiesel with different molar ratios of ammonia added. The purpose of argon molecules is to counteract the diluting effect caused by ammonia molecules so that the molar volumes of different systems are the same. The added argon molecules will not react with other species, and the interaction with other species is only through van der Waals forces [41]. To evaluate the effects of biodiesel on ammonia decomposition, system 10, containing only ammonia and argon, was constructed to compare with systems 7 to 9. The size of the simulation cubic box in each system is kept the same at 92.11 Å. All the molecules are placed randomly in the cubic box.

2.2. MD simulation details

All the simulations are performed using the Large-scale Atomic/Molecular Massively Parallel Simulator (LAMMPS) [42] with the $CHON_{2019}$ reactive force field parameters [43]. These parameters have been proven to be feasible to simulate the impact of adding ammonia on soot formation in ethylene flames [38], and they are verified in the simulation of the oxidation of PAHs by nitrogen-containing oxidants (NO and NO_2) [41]. ReaxFF force field eschews explicit bond switching to bond orders, which allows for continuous bond formation or breaking [44]. All the connectivity-dependent terms, i.e., bond, angle and torsion, are made bond order dependent so that their contributions diminish on bond breaking. The force field parameters of ReaxFF are calculated from quantum mechanics (QM) calculation and then trained extensively, including those relevant to the chemical space, such as the bond and angle stretches, activation and reaction energies, equation of state, and surface energies. ReaxFF is thus feasible for large-scale reactive systems, with similar accuracy to QM but significantly lower computational costs.

Each system was optimised geometrically using the Dreiding force field before the simulation [45]. The total simulation time for each system is set up to be 3 ns with a 0.1 fs time step. NVT ensemble (with a fixed number of atoms, box volume and system temperature) is used in all the simulations in conjunction with the Nosé-Hoover thermostat employing a damping constant of 10 fs (100 timesteps). The bonding formation and dynamic trajectory are recorded every 0.25 ps. For species analysis, a 0.3 bond strength cut-off is chosen in the post-processing to recognise the formation of molecules. A low cut-off value helps capture all the reactions, including even short-lived intermediate species. The simulation results were visualised by using OVITO Pro [46]. The ReacNetGenerator package developed by Zeng et al. [47] was used to derive the reaction pathways from the bonding information and atomic coordinates.

Table 1
Detailed system constructions.

No. system	Content	Density (g/cm^3)	Cubic box length (Å)
S_1	300MB + 1000Ar	0.150	92.11
S_2	300EP + 1000Ar	0.150	
S_3	300MC + 1000Ar	0.149	
S_4	300MB + 500Ar + 500NH_3	0.126	
S_5	300EP + 500Ar + 500NH_3	0.126	
S_6	300MC + 500Ar + 500NH_3	0.124	
S_7	300MB + 1000NH_3	0.101	
S_8	300EP + 1000NH_3	0.101	
S_9	300MC + 1000NH_3	0.100	
S_{10}	300Ar + 1000NH_3	0.062	

3. Results and discussion

3.1. Pyrolysis of biodiesel

Extensive simulations have been performed to examine the pyrolysis of different biodiesel surrogates. The simulation lasted for 80 ps at a

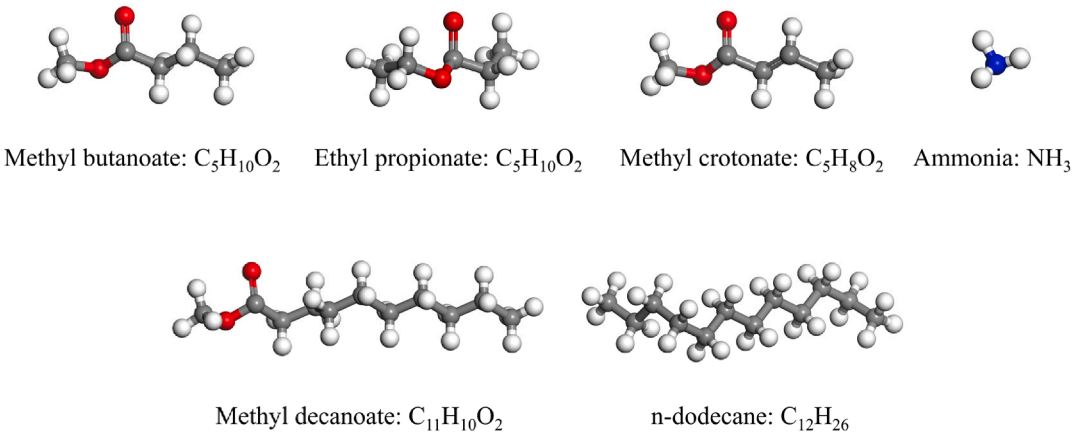

Fig. 1. The molecular structures and chemical formulas of biodiesel surrogates, n-dodecane, and ammonia (C, gray; H, white; O, red; N, blue).

constant temperature of 2800 K for all the surrogates, where the high temperature was used to speed up the reactions so that they can take place in reactive MD simulations. All the surrogate fuels have completed initial decomposition during this period, and there are no intact fuel molecules in the system. Fig. 2 shows sample results of pyrolysis of the three surrogates: MB, EP and MC, focusing on analysing the initial decomposition pathways of the fuel and the formation of C_1-C_2 unsaturated hydrocarbon products, which are highly correlated with the formation of PAHs as soot precursors. The reaction pathways shown in Fig. 2 display the effect of chemical structure on the pyrolysis of different biodiesel surrogates. The time evolution of the typical products is shown in Fig. 3. The oxygenated products CO and CO_2 were used to measure the carbon fixation capacity of oxygen atoms in biodiesel. More CO_2 indicates fewer esters to remove carbon atoms from the soot precursors, as two oxygen atoms are needed to fix one carbon atom, while CO only needs one. Formaldehyde (CH_2O) is highly relevant to the formation of CO through the reactions $CH_2O \rightarrow \cdot CHO \rightarrow CO$. Methoxy ($CH_3O\cdot$) radical is a key reactant in the formation of ·OH, while H_2O is used to measure the yield of ·OH. The amount of ·OH reflects the degree of oxidation occurring in the reaction system. The time evolutions of hydrocarbon species ethyne (C_2H_2) and propargyl ($\cdot C_3H_3$) radical are shown, as they are involved in the formation of initial pentagonal ring cyclopentadienyl (C_5H_5) [48] and six-membered ring benzene (C_6H_6) [49]. The product quantity remains relatively constant at the end of the simulation. The results are from the simulations of systems 1 to 3.

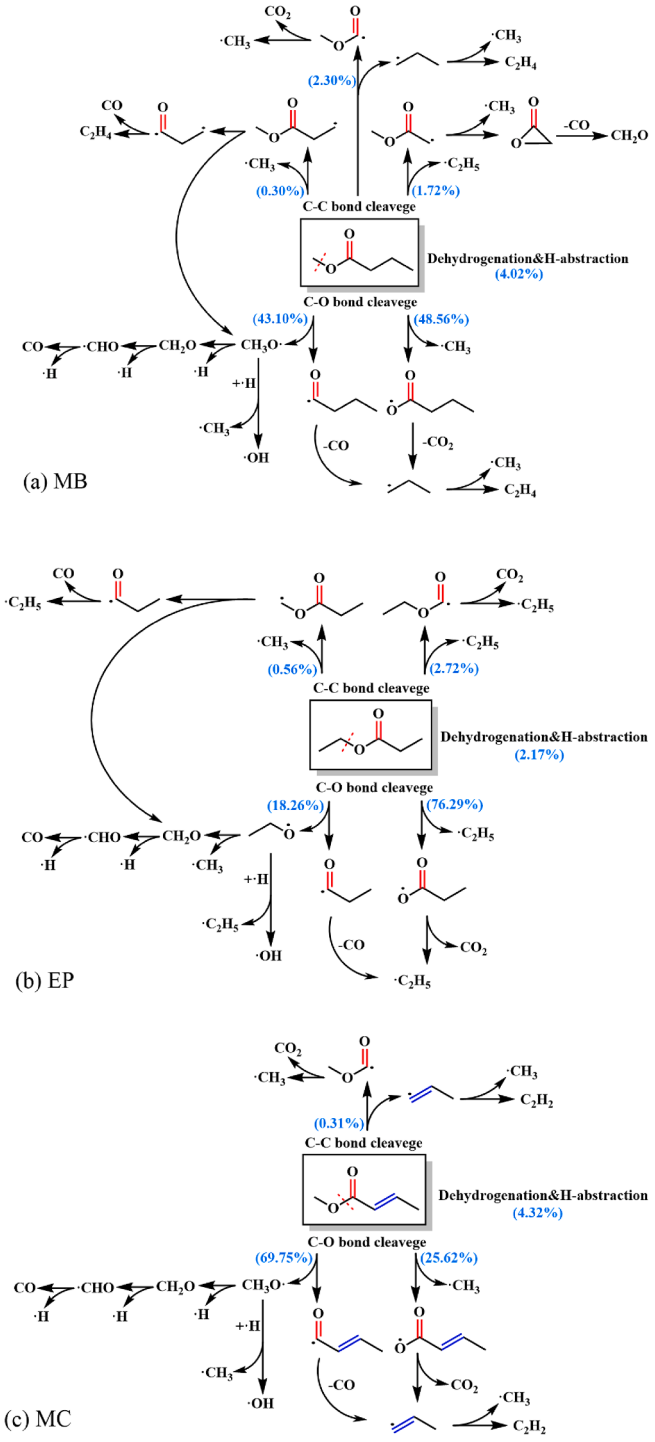

Fig. 2. Initial reaction pathways of (a) MB, (b) EP, and (c) MC pyrolysis under 2800 K, where the light blue percentage represents the proportion of this pathway to the total first-step decomposition pathways, the red dashed line on the fuel represents the bond that is most likely to break in the first step of the fuel pyrolysis.

The initial decomposition of different surrogates is mainly through the cleavage of C-O bonds. Only a small fraction of the fuel decomposition is triggered by breaking C-C bonds in all the systems, especially for MC (0.31%). For MB, the first step of C-O bond cleavage is more likely to generate $\cdot CH_3$ radicals (48.56%), followed by the production of CO_2. The probability of the outermost C-O bond breaking first in MB is 43.10%, resulting in the formation of $CH_3O\cdot$ and $\cdot C_4H_7O$. Then $\cdot C_4H_7O$ would release CO to form propyl radicals. The CO could also be produced through the continuous dehydrogenation of $CH_3O\cdot$, which accounts for the sustained increase in the amount of CO. For EP, the initial reaction primarily involves breaking C-O bonds to produce ethyl ($\cdot C_2H_5$) radical and $\cdot C_3H_5O_2$ (76.29%), and then the decomposition of $\cdot C_3H_5O_2$ would produce CO_2 and $\cdot C_2H_5$. Only 18.26% of EP would decompose into $\cdot C_2H_5O$ and $\cdot C_3H_5O$, and the subsequent reaction of $\cdot C_3H_5O$ would produce CO and $\cdot C_2H_5$. This is the reason why EP produces significantly more CO_2 than CO, as shown in Fig. 3a. There is some similarity in the reaction pathways of MC and MB, but MC tends to produce $CH_3O\cdot$ preferentially as an initial step (69.75%). As shown in Fig. 3a, during MC pyrolysis, the peak value of $CH_3O\cdot$ number reached 91, while in MB the value was 60, and only a small amount of $CH_3O\cdot$ was produced in EP. This could explain why MC is most prone to generating CO among all the surrogate fuels. The isomerisation of ethyl ester facilitates the formation of CO_2, while the carbon-carbon double bonds in MC facilitate the formation of CO.

The initial pyrolysis of MB mainly produces hydrocarbons such as $\cdot CH_3$ and ethylene (C_2H_4), while EP mainly produces $\cdot C_2H_5$, then $\cdot C_2H_5$ would quickly form C_2H_4 through a dehydrogenation reaction. MC mainly produces $\cdot CH_3$ and C_2H_2 due to the existence of carbon-carbon double bond. C_2H_2 will be added to the active site on the aromatic molecule generated by the abstraction of a gaseous hydrogen atom in the process of soot generation as that described by the H-abstraction-C_2H_2-addition (HACA) mechanism [50]. As shown in Fig. 3b, among MB, EP and MC, the carbon-carbon double bond in MC facilitates more effectively than isomerisation on generating C_2H_2 and resonance-stabilised radical propargyl ($\cdot C_3H_3$). Propargyl is known as the key precursor in benzene formation via $\cdot C_3H_3 + \cdot C_3H_3 \rightarrow C_6H_6$. C_2H_2 would combine with $\cdot C_3H_3$ to form cyclopentadienyl (C_5H_5), a key initiator of soot formation in the clustering of hydrocarbons by the radical chain reactions model [48]. The ·OH radicals are produced through the reactions $CH_3O\cdot + \cdot H \rightarrow CH_3OH$ and $CH_3OH \rightarrow \cdot CH_3 + \cdot OH$ in MB and MC systems, with MC producing more ·OH. For EP, only 18.26% of its initial decomposition produces $\cdot C_2H_5O$, which subsequently generates ·OH. Therefore, EP produces a lower amount of ·OH during its decomposition. The lower amount of ·OH produced during the decomposition of EP indicates the presence of fewer oxidative reactions. This can explain why fewer dehydrogenation and H-abstraction reactions (2.17%) occur in the decomposition of EP, whereas the corresponding percentages for MB and MC are 4.02% and 4.23%, respectively. It is worth noting that the quantities of C_2H_2 and $\cdot C_3H_3$ in EP were initially low before 0.76 ns but

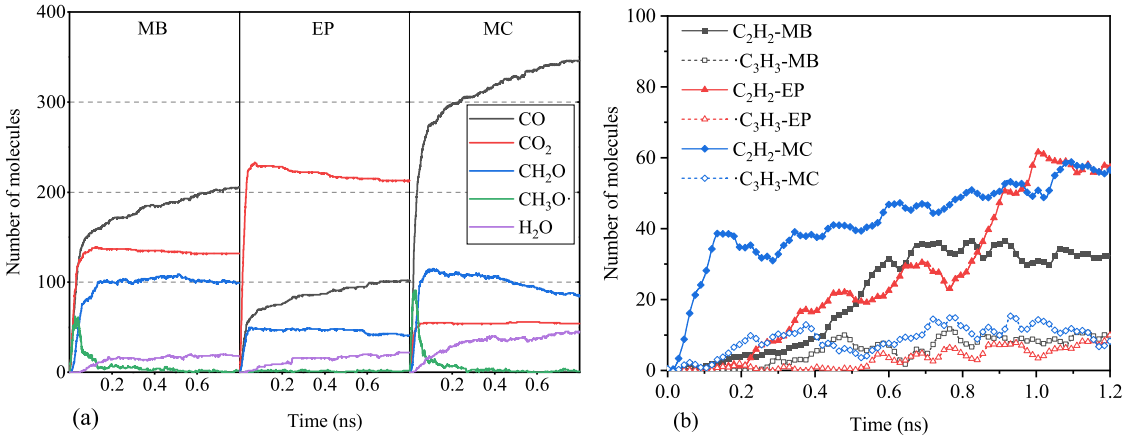

Fig. 3. (a) Time evolution of the typical oxygenated products; (b) comparison of different fuel surrogates on the time evolution of C_2H_2 and $\cdot C_3H_3$.

then progressively increased to almost the same level as MC. This can be attributed to the weaker ability of the oxidation groups (mainly ·OH) in EP to oxidise the soot precursors. The increased production of ·OH during the decomposition of MC results in a higher water yield, as illustrated in Fig. 3a.

The first-order kinetics equation can be utilised to determine the rate constant at a constant temperature in reactive MD simulations by substituting the concentration of the reactant with the number of reactant molecules (N_t). The equation is expressed as follows:

$$\ln N_t - \ln N_0 = -kt \tag{1}$$

The slope and y-intercept of the linearly fitted Arrhenius plots of rate constant are employed to calculate the global activation energy (E_a) and the pre-exponential factor (A) in the equation given as:

$$\ln k = \ln A - \frac{E_a}{RT} \tag{2}$$

where R is the universal gas constant. The activation energy of biodiesel fuel surrogates and DDC is summarised in Table 2. The reliability of ReaxFF MD simulations in calculating the activation energy of fuels at high temperatures by comparing them with the values obtained from low-temperature experiments has been validated in previous modeling studies [51–53]. In this study, the calculated activation energy of MDN (47.19 kcal/mol) at a relatively high temperature (2200–3000 K) also fits well with the experimental results (47.3 kcal/mol) obtained at a lower temperature (1262–1388 K) [54], indicating a correlation between the results of high-temperature simulation and low-temperature experiment. The calculated activation energy of MB is 39.28 kcal/mol, which fits well with the experimental result (38.9 kcal/mol) obtained under the high pressure environment. The reaction with lower activation energy is more likely to occur under the same conditions. The activation energy of MDN is lower than DDC, indicating that the ester function groups facilitate the pyrolysis. The activation energy of MDN is higher than MB, which means the long alkane chain in FAMEs would make the initial decomposition reaction more difficult to occur. The isomerised ethyl ester of EP and the unsaturated methyl ester of MC correspond to a lower activation energy. MC decomposes most easily among all the simulated fuels.

As shown in Fig. 4, the pyrolysis rate of MDN is about 1.47–4.24 times higher than DDC, and the difference between DDC and MDC decreases with temperature increase, which indicates that the effect of the ester group on fuel pyrolysis is more prominent at lower temperatures. This trend is also observed in other fuels such as MB, EP and MC, as the isomerisation of the ethyl ester of EP and the double bond in MC can facilitate the pyrolysis, and the difference narrows in higher temperatures.

Table 2
Comparison of the activation energy of the fuel surrogates of biodiesel and n-dodecane.

Fuel	DDC	MDN	MB	EP	MC
Ea (kcal/mol)	60.37	47.19	39.28	34.79	32.49

3.2. The promotion of ammonia reactions by biodiesel decomposition

By comparing systems 7 to 9 and 10, it can be seen from Fig. 5a that adding MB, EP, and MC is beneficial to promoting the decomposition of ammonia, but the effectiveness of promotion is different, with MC > MB > EP in descending order. This trend is inconsistent with the decomposition rates of MB, EP, and MC. As displayed in Table 2, the activation energy is of the order of MC < EP < MB, so that the decomposition rates of these biofuels follow the trend MC > EP > MB, as shown in Fig. 5a. These biodiesel surrogates promote the decomposition of ammonia mainly because their rapid decomposition in a short time (80 ps) creates a pool of abundant free radicals, with MC creating the most favourable free radical environment for ammonia decomposition. As shown in Fig. 5b, when no biodiesel is added, the direct decomposition of ammonia into amido ($\cdot NH_2$) or imidogen (:NH) radical is the main consumption pathway of ammonia, followed by the abstraction reactions by $\cdot N_2H$,:NH, $\cdot NH_2$, N_2, and ·H. The addition of biofuel produces oxygen-containing products such as $CH_3O\cdot$, ·OH, $CH_3CH_2O\cdot$, NO and carbon-containing species such as $\cdot C_2H_5$, $\cdot CH_3$, and CN. These species provide new reaction pathways for the consumption of ammonia.

The net flux reaction frequency (forward–reverse) of ammonia with carbon-containing and oxygen-containing species is shown in Fig. 6, where the frequency refers to number of counts. The H-abstraction reaction of ammonia by $CH_3O\cdot$ is the primary reaction in MB/MC-NH_3 systems. The reaction between $CH_3CH_2O\cdot$ and ammonia is only observed in the EP-NH_3 system. The reaction between $CH_3O\cdot$ and ammonia in this system is negligible. The reaction frequency between ·OH and ammonia in the MC-NH_3 system is slightly higher than that in the MB-NH_3 system, while in the EP-NH_3 system, the frequency of this reaction is significantly lower than that in the other two systems. The reaction between $\cdot CH_3$ and ammonia occurs more frequently in the MB-NH_3 system, while a significant amount of reaction between $\cdot C_2H_5$ and ammonia is observed in the EP-NH_3 system. More CN would be produced in MB/MC-NH_3 systems and react with ammonia. The H-abstraction reaction of oxygen-containing products (mainly $CH_3O\cdot$ and ·OH) released in the biodiesel system with ammonia is the main driver of ammonia consumption, while the reaction of carbon-containing products with ammonia also contributes to ammonia consumption to some extent.

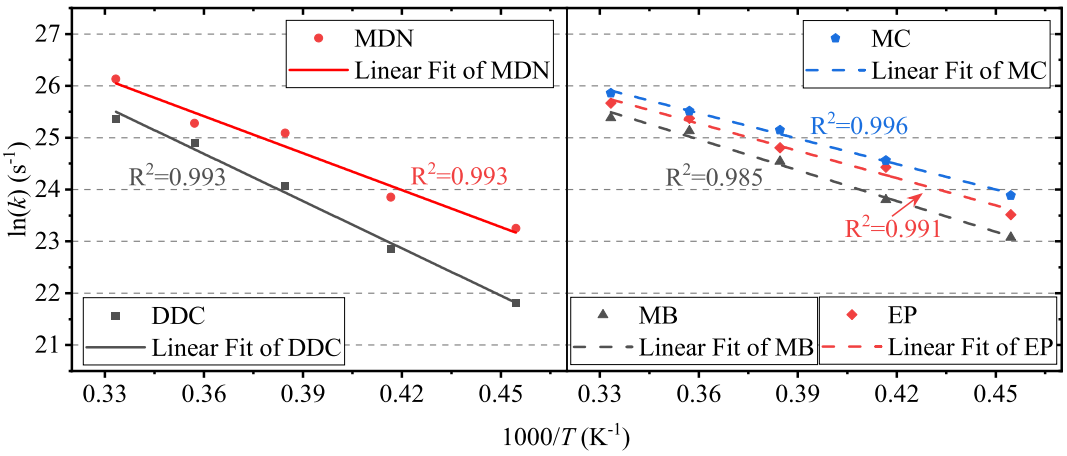

Fig. 4. Fitted rate constants of DDC, MDN, MB, EP and MC versus inverse temperature from ReaxFF MD simulations.

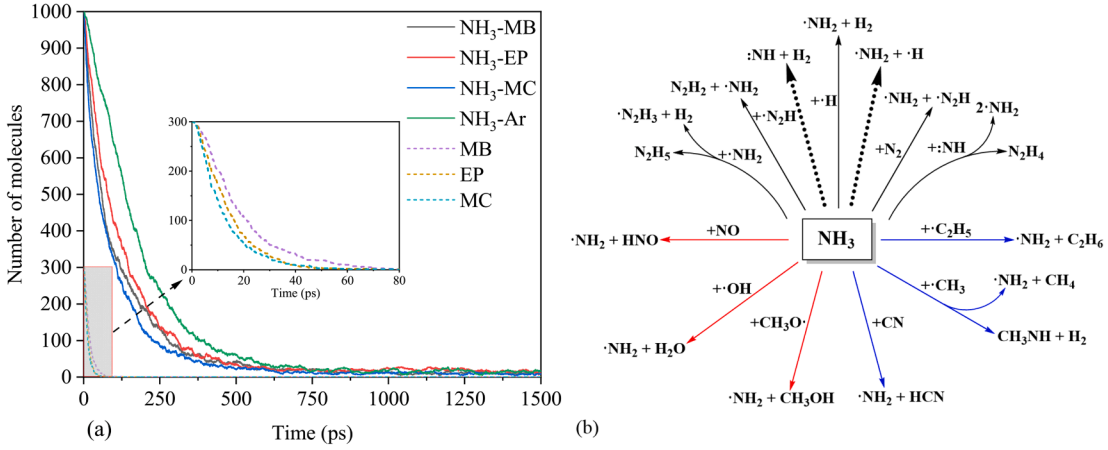

Fig. 5. (a) Time evolution of the numbers of NH_3 and MB/EP/MC molecules in different systems at 2800 K, where the solid line represents the evolution of NH_3 in different systems, the short dash line represents the different biodiesel surrogates; (b) reactions of NH_3 in different systems, where the black line indicates the reactions occurred in all the systems, the red line represents the reactions of NH_3 with oxygen-containing species, the blue line represents the reactions of NH_3 with nitrogen-containing species.

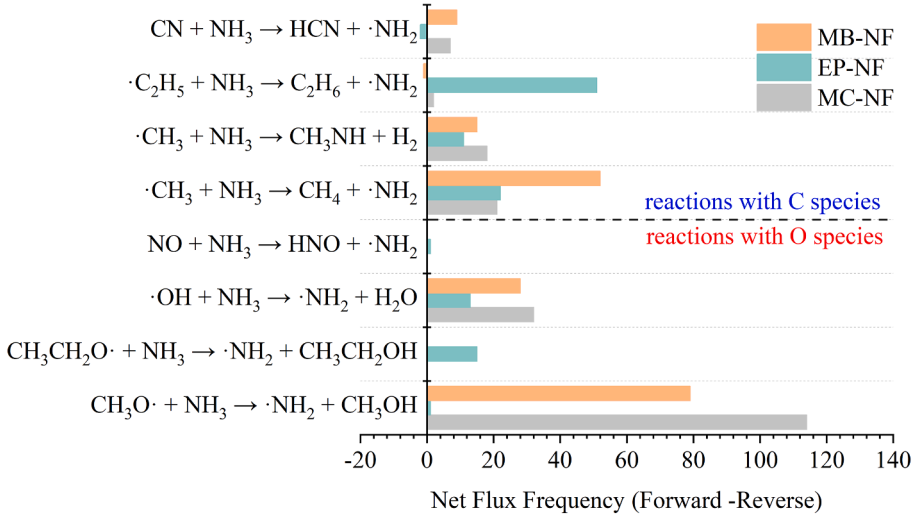

Fig. 6. Net flux reaction frequency of NH_3 with carbon-containing and oxygen-containing species in MB/EP/MC-NH_3 systems.

3.3. The NO production of ammonia-biodiesel co-pyrolysis

As oxygen atoms exist in biodiesel fuels, the interactions of the oxygen-containing products produced by biodiesel pyrolysis would react with nitrogen-containing radicals produced by ammonia pyrolysis to form NO, NO_2, and N_2O, which are recognised as vital pollutants during the use of ammonia as a fuel. The quantities of NO_2 and N_2O generated were too small to be quantified and analysed effectively in the co-pyrolysis conditions without the presence of oxygen. Therefore, this study focused primarily on analysing the formation mechanism of NO. Fig. 7a displayed the maximum number of NO molecules produced in different systems under 2000 K, 2400 K, and 2800 K. The results are from the simulations of systems 7 to 9. The high temperature is found to promote the generation of NO. In the EP-NH_3 and MC-NH_3 systems, reducing the temperature from 2800 K to 2400 K resulted in a 50% decrease in the production of NO. There is no NO produced in the EP-NH_3 system under 2000 K. The trend of NO generation is MC > MB > EP. The NO formation pathways are shown in Fig. 7b, based on the analysis of the reactive MD results. The mechanism of NO generation is consistent in both the MB-NH_3 and MC-NH_3 systems. The $CH_3O\cdot$ released by MB or MC would react with $\cdot NH_2$ radicals produced by ammonia to form CH_3ONH_2. This reaction is observed 37 times in MC-NH_3 systems and 20 times in MB-NH_3 systems. CH_3ONH_2 would first release $\cdot CH_3$ radicals to form $H_2NO\cdot$, and $H_2NO\cdot$ would direct decompose or experience a series of dehydrogenation or H-abstraction reactions to form NO. Another pathway is the fellow-up reactions of $CH_3O\cdot$, which would produce ·OH. Then the H_3NO would be produced through the reaction $\cdot OH + \cdot NH_2 \rightarrow H_3NO$. This reaction happened 72 times in the MC-NH_3 system and 50 times in the MB-NH_3 system. This reaction is also found 19 times in EP-NH_3 systems because the follow-up reactions of $C_2H_5O\cdot$ produce the ·OH. H_3NO would release an ·H radical to form $H_2NO\cdot$. $H_2NO\cdot$ would produce NO following the reactions discussed previously. By comparing systems 4 to 6 and 7 to 9, it was observed that as more ammonia was mixed with the biodiesel surrogate, there was a tendency to produce more NO, which was particularly evident in the MC-NH_3 system. Because adding more ammonia leads to the generation of more $\cdot NH_2$ radicals, which then react with oxygen-containing radicals to produce more NO through subsequent reactions.

It can be seen from Fig. 8 that the consumption and production pathways of NO are mainly through the reaction $\cdot H + HNO \leftrightarrow NO + H_2$ (R_1) in different systems. Then the direct decomposition of $H_2NO\cdot$ (R_4) and HNO (R_2) is also the primary pathway for NO formation. The generation and consumption of NO are most active in the MC-NH_3 system, followed by the MB-NH_3 system, and least active in the EP-NH_3 system. There are 11 times reactions of H-abstraction reactions of HNO by ·OH observed in the MC-NH_3 system, while there are no such reactions in the other systems.

3.4. The effects of ammonia on soot incipient of biodiesel

To investigate the biodiesel soot reduction mechanism by ammonia addition, we used a relatively high temperature (3000 K) to speed up the reactions. Using a high temperature in ReaxFF is a common strategy and is thought only to affect the reaction rate rather than the reaction pathways [55], although more systematic assessments might be needed to test this assertion used in reactive MD. Fig. 9 shows the maximum numbers of ·H and ·OH radicals found during the simulations in different systems. Pure MC decomposition tends to produce the most ·OH and the

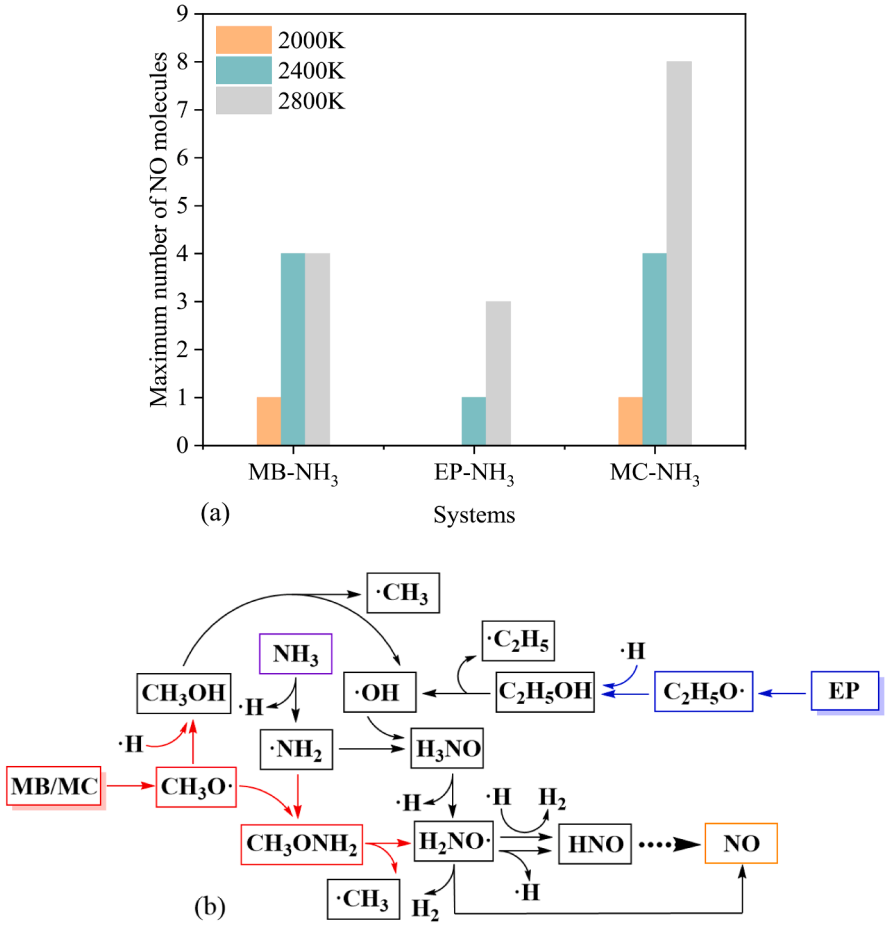

Fig. 7. (a) Maximum number of NO molecules in different systems at 2000 K, 2400 K, and 2800 K; (b) reaction pathways of NO formation in MB/EP/MC-NH_3 systems.

Reaction pathways of NO :

R_1 ·H + HNO ↔ NO + H_2

R_2 HNO ↔ NO + ·H

R_3 HNO + ·NH_2 ↔ NO + NH_3

R_4 H_2NO· ↔ NO + H_2

R_5 HNO + ·N_2H ↔ NO + N_2H_2

R_6 HNO + ·OH ↔ NO + H_2O

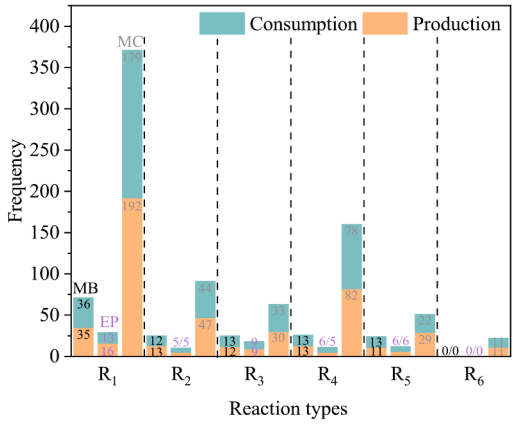

Fig. 8. Frequency of consumption and production pathways of NO in MB/EP/MC-NH_3 systems under 2800 K.

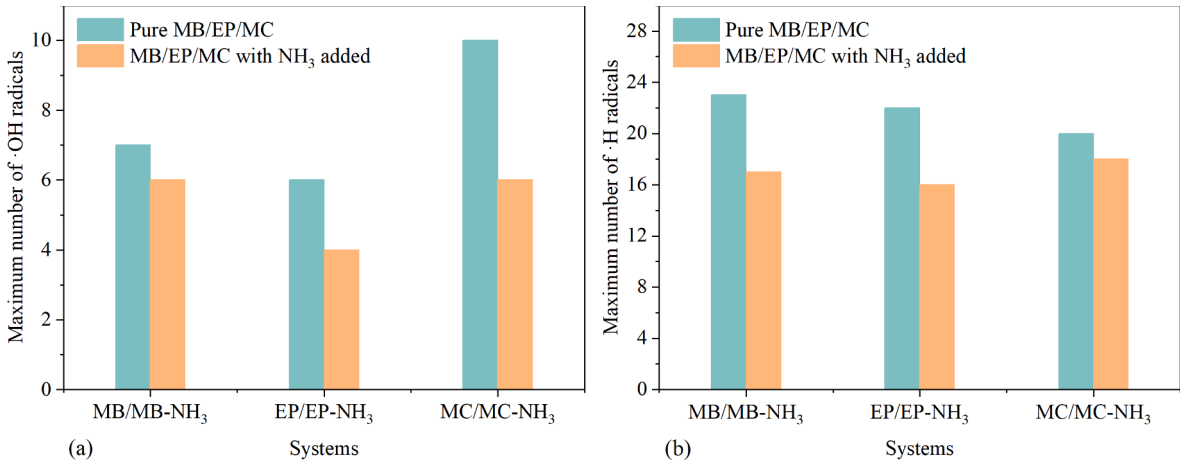

Fig. 9. Maximum number of free radicals (a)·OH and (b)·H in different systems.

least ·H radicals. The addition of ammonia would create new reaction pathways to consume ·H and ·OH. Thus, the maximum numbers of ·H and ·OH in each system are reduced. The decrease in ·OH implies that the addition of ammonia weakens the oxidation process of soot. This finding is consistent with the conclusion from Cheng et al. [23]. Zhang et al. [56] carried out an experimental study and kinetic modelling and concluded that the decrease in ·H would decrease the HACA reaction rate, which could be the main reason for the reduced soot formation. This is consistent with our simulation results.

Fig. 10 shows the time evolution of the sum of the carbon number of molecules with a carbon number greater than ten, indicating that the molecules tend to form incipient soot. This strategy was established

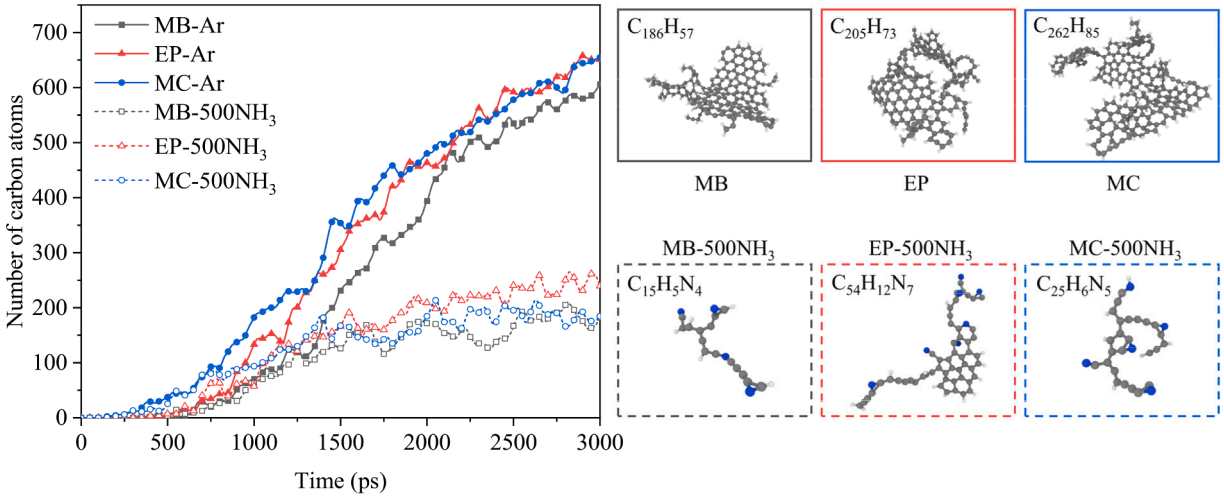

Fig. 10. Time evolution of the sum of the carbon number of molecules with carbon number greater than ten at 3000 K and the largest molecule at different systems at 3 ns.

based on the analysis from Zhang et al. [38], who suggested that aromatic precursors larger than naphthalene ($C_{10}H_8$) would gradually form soot nanoparticles over time scales that surpass the duration of the ReaxFF MD simulation. To reduce computation errors and guarantee that the simulation is statistically accurate, each case is averaged three times with varying initial velocities and atomic coordinate distributions. Among all the biodiesel surrogates, MC has the highest tendency to form molecules with carbon numbers greater than 10, followed by EP, while MB consistently has the lowest total carbon content for molecules with carbon numbers exceeding 10 throughout the entire simulation period. The largest molecule found in the MC-Ar system is $C_{262}H_{85}$, while the corresponding molecule is $C_{205}H_{73}$ in EP-Ar and $C_{186}H_{57}$ in MB-Ar systems, respectively.

The addition of ammonia to biodiesel can efficiently reduce soot formation. By comparing systems 7 to 9 with systems 1 to 3, it was found that when biodiesel is mixed with 1000 ammonia molecules, almost no molecules with carbon above ten are produced at the end of the simulation (3 ns). For biodiesel pyrolysis in the presence of 500 molecules of ammonia (systems 4 to 6), a certain quantity of molecules with a carbon number larger than ten are still created at the end of the simulation, but the amount of these molecules produced is dramatically reduced compared to the pure biodiesel system (systems 1 to 3) as shown in Fig. 10. However, before 750 ps, there was no significant decrease in the total carbon content of molecules with carbon numbers exceeding ten. Even more molecules with carbon number above ten are produced in the EP-NH_3 system than in the EP-Ar system. This may be attributed to the fact that ammonia can also promote the decomposition of biodiesel to a certain extent. A faster decomposition rate means that the unsaturated hydrocarbons generated by the pyrolysis of biodiesel will recombine in a shorter time. The rate of ammonia decomposition is slower than that of biodiesel decomposition. Therefore, during the process of initial biodiesel decomposition to form unsaturated hydrocarbons and their combination to form soot precursors, the inhibitory effect of ammonia decomposition products on soot generation is not significant. This is consistent with the findings of Cheng et al. [23], who reported that the addition of ammonia has a more powerful inhibitory effect on larger PAH A_4 (pyrene) than on smaller ones, such as A_1 (benzene), A_2 (naphthalene), and A3 (anthracene), during soot formation. It should be noted that one of the limitations of this work is that the inclusion of ammonia would reduce the flame temperature of biodiesel in reality, which could lead to a decrease in soot production, but this is not accounted for in the reactive MD simulations.

Interestingly, ammonia has a more substantial inhibitory effect on soot generation in MC than in EP. In the absence of ammonia, MC exhibits a more pronounced trend in soot production than EP. However, with the addition of ammonia, MC produces less soot than EP. At the end of the 3 ns simulation, the largest molecule produced in the MC-NH_3 system is $C_{26}H_6N_5$, which contains only one pentagonal carbon ring, and this state is still in the early stages of soot growth. On the other hand, the largest molecule produced in the EP-NH_3 system is $C_{54}H_{12}N_7$, a PAH-like molecule that already contains several five-membered and six-membered carbon ring structures. After the addition of ammonia, the molecules with carbon atoms above ten produced in MB system decreased by 70.13%. The corresponding values for the EP and MC systems were 63.32% and 71.98%, respectively.

The reaction pathway analysis shows that nitrogen-containing elements mainly combine with C_1-C_3 unsaturated hydrocarbons in the form of $\cdot NH_2$, and NH is only found to combine with $\cdot CH_3$. The frequency of $\cdot NH_2$ combination with C_1-C_3 hydrocarbon species in different systems is shown in Fig. 11. Among all systems, $\cdot NH_2$ primarily reacts with $\cdot CH_3$, with the highest binding frequency observed in MB and the lowest in EP. In the EP-NH_3 system, $\cdot NH_2$ mainly reacts with C_2 species, and only a small amount of $\cdot C_3H_3$ and C_3H_4 were found to react with $\cdot NH_2$. However, in the MC-NH_3 system, a significant amount of reactions of $\cdot NH_2$ react with $\cdot C_3H_3$, C_3H_4, and $\cdot C_3H_5$ were observed. In the MB system, C_2H_4 is the main form of C_2 hydrocarbon species binding with $\cdot NH_2$, whereas C_2H_2 is the primary form in the MC system. In the EP system, the binding frequencies of $\cdot NH_2$ with C_2H_2 up to $\cdot C_2H_5$ are similar. In addition, the total amount of reactions of $\cdot NH_2$ reacts with unsaturated hydrocarbons occurred 211 times in the MC-NH_3 system, while it only occurred 164 times in the EP-NH_3 system and 193 in the MB-NH_3 system.

Fig. 12 shows the time evolution of some typical species related to soot inhibition, including $\cdot NH_2$, $\cdot CH_3$, HCN, and C_2H_2. It can be seen that among all systems, the production and consumption rates of $\cdot NH_2$ are the highest in the MC-NH_3 system, while this rate is the lowest in the EP-

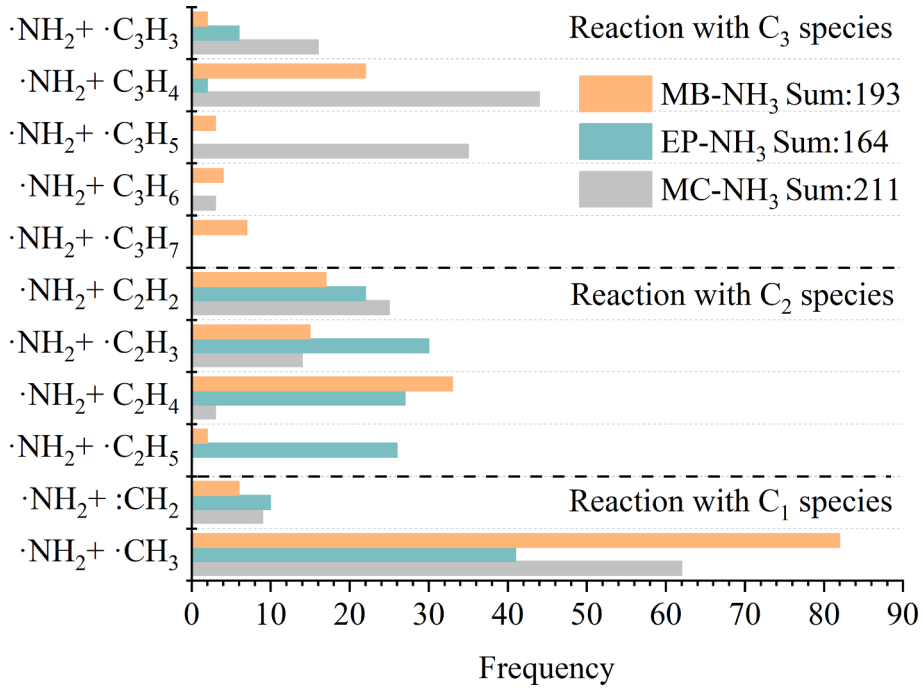

Fig. 11. Frequency of the addition reactions of $\cdot NH_2$ radicals with C_1, C_2, and C_3 hydrocarbon species in MB/EP/MC-NH_3 systems.

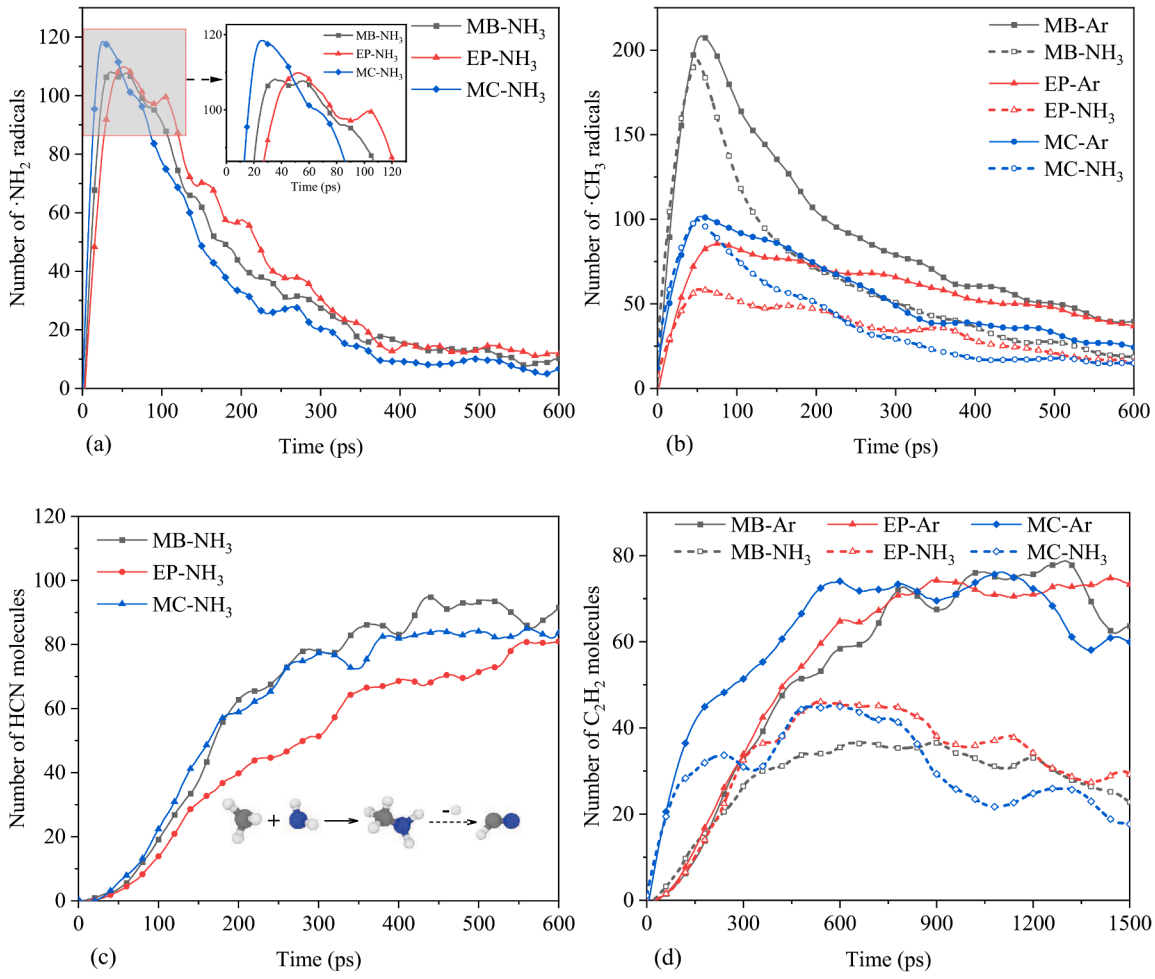

Fig. 12. Time evolution of the number of (a) ·NH_2, (b) ·CH_3 radicals, (c) HCN, and (d) C_2H_2 molecules at 3000 K.

NH_3 system. This is because, on the one hand, as discussed in section 3.2, compared to EP, the decomposition of MC creates a more favourable radical-rich environment for ammonia reactions, resulting in the release of more ·NH_2. On the other hand, the decomposition products of MC have lower saturation due to the existence of a carbon–carbon double bond, making them more reactive with ·NH_2.

HCN is thought of as a key product that can prevent carbon atoms from forming soot. There are two main pathways for HCN formation. Pathway1 is firstly through the reaction·CH_3 + ·NH_2 → CH_3NH_2 to form CH_3NH_2, then CH_3NH_2 would experience a series of dehydrogenation and H-abstraction reactions to form HCN. Pathway 2 first involves the decomposition of ·CH_3 into:CH_2 and ·H, followed by the combination of: CH_2 with ·NH_2 to form ·CH_2NH_2, subsequently leading to the formation of HCN. ·CH_3 is the primary reactant in both of these pathways, and its concentration directly influences the production of HCN. The decomposition of MB tends to produce the highest amount of ·CH_3, with a peak value of 208, followed by MC, with a peak value of 102, and the least is EP, with a peak value of 85. When ammonia was added to these systems, ·CH_3 radicals were reduced. However, the peak value in the MC-NH_3 system does not show a significant change, while the peak value in the EP-NH_3 system noticeably decreases. This is because CH_3O· produced by MB or MC would react with ammonia through the reaction CH_3O· + NH_3 → CH_3OH + ·NH_2 to form CH_3OH, and then CH_3OH decomposes into ·CH_3 and ·OH. As discussed before, MC would produce more CH_3O· compared to MB. Therefore, the peak value of ·CH_3 does not decrease in the MC-NH_3 system. Almost no CH_3O· was produced during the pyrolysis of EP, so the peak value of ·CH_3 decreased significantly, leading to the lower production of HCN in the EP-NH_3 system.

C_2H_2 is a crucial precursor during soot formation. Adding ammonia reduces the amount of C_2H_2 produced, but the time at which C_2H_2 starts to reduce varies in different systems. In the MC-NH_3 system, C_2H_2 first reaches the inflexion point at 63.2 ps, followed by MB at 203.6 ps and EP at 302.8 ps. Reducing the concentration of C_2H_2 in a shorter time helps reduce soot formation. Further experimental support is needed to confirm the detailed kinetic mechanisms revealed by the reactive MD.

The detailed mechanism of soot reduction in MB/EP/MC-NH_3 systems is summarised in Fig. 13. Firstly, the function of oxygen atoms is clarified. During the decomposition processes of MB, EP, and MC, CO or CO_2 will be released. This part of carbon atoms fixed by oxygen atoms will not participate in soot formation. The pyrolysis of MB and MC would produce CH_3O· radicals, while the decomposition of EP would produce C_2H_5O· radicals. These radicals will undergo hydrogenation, and then the carbon-oxygen bonds will break to form ·OH. The produced ·OH would combine with certain hydrocarbons (C_1-C_3) to form structurally stable alcohol species or oxidise these hydrocarbons and produce CO. The CH_3O· and C_2H_5O· will also produce CO through stepwise decomposition reactions.

Secondly, nitrogen also plays an essential role in reducing soot. Ammonia can directly decompose or react with the ·H or ·OH to form ·NH_2 and:NH radicals. These radicals will combine with C_2-C_3 hydrocarbons generated from the decomposition of biodiesel to form C_2-N and C_3-N species. The N atoms occupy the active sites of these carbonaceous precursors and slow down their combination to form incipient soot. ·NH_2 would combine with:CH_2 or ·CH_3 to form ·CH_2NH_2 or CH_3NH_2, while:NH is found only to blend with ·CH_3 to form CH_3NH. These C_1-N species would experience dehydrogenation reactions to form HCN and

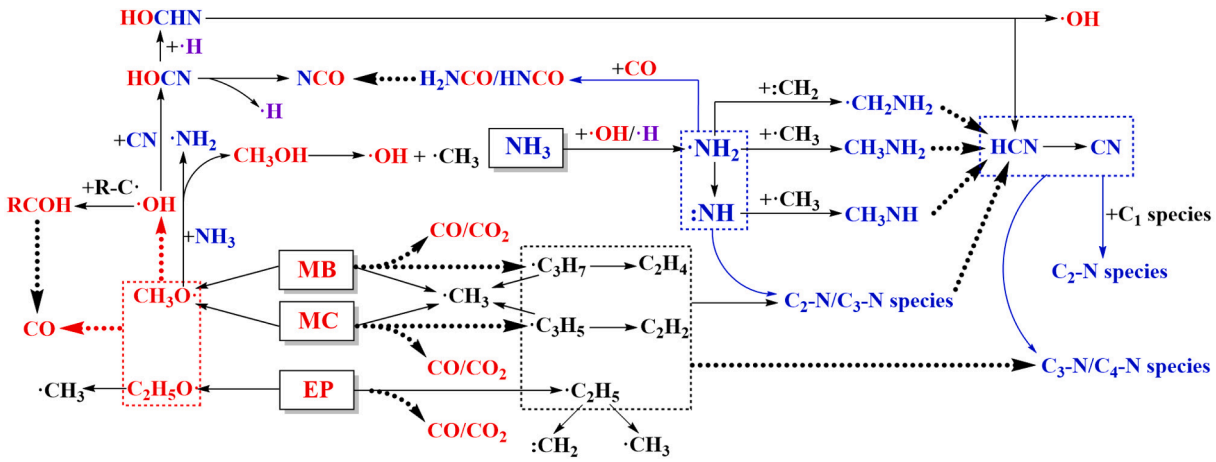

Fig. 13. Mechanism of soot reduction in MB/EP/MC systems with ammonia added, where the red letters represent oxygen-containing products, the blue letters represent nitrogen-containing products, the black letters represent hydrocarbons, and the purple letter represents ·H radical. A straight line indicates that a substance undergoes a one-step reaction to produce another substance, while a bold dashed line indicates that a substance undergoes a multi-step reaction to produce another substance.

CN. HCN and CN would also participate in the reactions with C_1-C_3 hydrocarbons to form C_2-C_4-N species. It needs to be noticed that the C_2-N and C_3-N products can also generate HCN and CN, but HCN and CN are mainly produced by the dehydrogenation of C_1-N products.

Finally, nitrogen and oxygen atoms synergise in fixing carbon atoms. The ·OH would react with CN to form HOCN, and HOCN would release a ·H to form NCO or add a ·H to form HOCHN, which finally decomposes to ·OH and HCN. $·NH_2$ or:NH produced by ammonia would combine with CO to form H_2NCO or HNCO, finally converting to NCO. $CH_3O·$ would react with ammonia to form CH_3OH, then release $·CH_3$, participating in the formation of HCN. The molecular structure of typical C_2-C_4-N species, alcohols, and the products of carbon fixation through the synergistic action of nitrogen and oxygen are shown in Table 3. The nitrogen-containing tricyclic structure found in this study was also observed in previous simulations [38]. The products contain numerous nitrogen-containing heterocycles, where nitrogen occupies two active sites on carbon atoms, effectively reducing soot formation.

4. Conclusions

In this study, the pyrolysis of different biodiesel surrogates, the promoting effect of biodiesel decomposition on ammonia reactions, the issue of NO generation during the ammonia-biodiesel reaction process, and the mechanism of ammonia inhibition of soot formation during biodiesel pyrolysis were investigated using ReaxFF-based MD simulations. The results of MD revealed the atomic-scale chemical processes involved.

Compared to alkanes, the presence of ester groups lowers the activation energy of the reaction. The shorter chain length, isomerisation, and carbon-carbon double bond in biodiesel effectively reduce the reaction activation energy of biodiesel. The presence of carbon-carbon double bonds increases the likelihood of soot formation. However, the existence of double bonds facilitates the generation of more oxidising groups (mainly $CH_3O·$ and ·OH) during MC decomposition. EP, which has ester groups located in the middle, tends to produce more soot due to the weak oxidising environment in the reaction system.

The coexistence of biodiesel and ammonia can effectively promote the decomposition of ammonia, as biodiesel completes the initial pyrolysis process first and releases small free radicals containing carbon or oxygen atoms, creating new reaction pathways for ammonia decomposition. However, different biodiesel structures have varying effectiveness of promoting ammonia reactions. MC containing double bonds creates the most enriched free radical environment and is most favourable for ammonia decomposition. EP exhibits a weaker promoting effect on ammonia decomposition than MB and MC.

High temperature promotes the occurrence of the reaction, and with

Table 3
Molecular structures and chemical formulas of typical C_2-N/C_3-N/C_4-N/Alcohols/O-RC-N species.

	Molecular structures				
C_2-N species	C_2HN	C_2H_2N	C_2H_3N	C_2N_2	C_2H_3N
C_3-N species	C_3N_2	C_3HN_2	$C_3H_2N_2$	C_3N_2	C_3H_3N
C_4-N species	C_4HN_2	C_4H_2N	C_4H_2N	C_4HN_2	C_4H_2N
Alcohols	CH_3OH	C_2HOH	C_2H_3OH	C_2H_2OH	C_3H_4OH
O-RC-N species	HNCO	HOCN	NCO	HOC_2N	HOCHN

increasing temperature, different types of biodiesel mixed with ammonia will generate more NO. The NO production during co-pyrolysis with ammonia is MC > MB > EP in descending order, as more $CH_3O\cdot$ and $\cdot OH$ would be produced to combine with NH_2 and finally converted to NO in the MC system. The main reaction pathway for NO production in each system is $\cdot H + HNO \rightarrow NO + H_2$, followed by the direct decomposition of HNO or H_2NO.

Adding ammonia can effectively reduce soot production during the pyrolysis of biodiesel, especially for MC. The presence of carbon-carbon double bonds in MC tends to generate more soot precursors, but when it is co-pyrolysed with ammonia, the formation of soot is significantly reduced. Because ammonia decomposes in the MC environment to produce $\cdot NH_2$ at the fastest rate, the low degree of saturation of the decomposition products of MC provides more binding sites for the $\cdot NH_2$ addition reaction, resulting in the quickest consumption rate of $\cdot NH_2$. In addition, the reaction of $CH_3O\cdot$ from MC decomposition with ammonia generates CH_3OH, which decomposes to produce $\cdot CH_3$, the primary reactant for HCN production. The increase in the concentration of $\cdot CH_3$ is favourable for producing more HCN, thereby reducing the carbon content entering the incipient soot. The high reactivity of the MC system causes the rapid suppression of the soot-forming species C_2H_2 in the least amount of time. The oxygen in biodiesel, nitrogen in ammonia, and the synergistic effect of oxygen and nitrogen all inhibit biodiesel soot formation.

This work provides new insights into the detailed reaction mechanisms of the co-pyrolysis of biodiesel and ammonia using reactive MD simulations. The chemical pathways identified from the MD simulation can be used to optimise the reaction conditions as well as the mixture compositions of ammonia-biodiesel blends, which can in turn guide the development of ammonia-biodiesel co-firing technology. Further MD simulations will be carried out in oxidant environments, which will provide molecular insights into the energy conversion process in practical devices such as combustors and engines.

CRediT authorship contribution statement

Zhihao Xing: Conceptualization, Investigation, Methodology, Software, Writing – original draft. **Cheng Chen:** Conceptualization, Investigation, Methodology, Software. **Xi Jiang:** Conceptualization, Funding acquisition, Methodology, Supervision, Writing – review & editing.

Declaration of Competing Interest

The authors declare that they have no known competing financial interests or personal relationships that could have appeared to influence the work reported in this paper.

Data availability

Data will be made available on request.

Acknowledgements

Supercomputing time on ARCHER is provided by the “UK Consortium on Mesoscale Engineering Sciences (UKCOMES)” under the UK Engineering and Physical Sciences Research Council Grant No. EP/R029598/1. This work made use of computational support by CoSeC, the Computational Science Centre for Research Communities, through UKCOMES.

References

[1] Valera-Medina A, Xiao H, Owen-Jones M, David WIF, Bowen PJ. Ammonia for power. Prog Energy Combust Sci 2018;69:63–102. https://doi.org/10.1016/j.pecs.2018.07.001.

[2] Al-Aboosi FY, El-Halwagi MM, Moore M, Nielsen RB. Renewable ammonia as an alternative fuel for the shipping industry. Curr Opin Chem Eng 2021;31:100670. https://doi.org/10.1016/j.coche.2021.100670.

[3] Olabi AG, Abdelkareem MA, Al-Murisi M, Shehata N, Alami AH, Radwan A, et al. Recent progress in green ammonia: production, applications, assessment; barriers, and its role in achieving the sustainable development goals. Energ Conver Manage 2023;277:116594. https://doi.org/10.1016/j.enconman.2022.116594.

[4] Zamfirescu C, Dincer I. Using ammonia as a sustainable fuel. J Power Sources 2008;185:459–65. https://doi.org/10.1016/j.jpowsour.2008.02.097.

[5] Dolan RH, Anderson JE, Wallington TJ. Outlook for ammonia as a sustainable transportation fuel. Sustainable Energy Fuels 2021;5:4830–41. https://doi.org/10.1039/D1SE00979F.

[6] Berwal P, Kumar S, Khandelwal B. A comprehensive review on synthesis, chemical kinetics, and practical application of ammonia as future fuel for combustion. J Energy Inst 2021;99:273–98. https://doi.org/10.1016/j.joei.2021.10.001.

[7] Cai T, Zhao D, Wang B, Li J, Guan Y. NO emission and thermal performances studies on premixed ammonia-oxygen combustion in a CO_2-free micro-planar combustor. Fuel 2020;280:118554. https://doi.org/10.1016/j.fuel.2020.118554.

[8] Boningari T, Smirniotis PG. Impact of nitrogen oxides on the environment and human health: Mn-based materials for the NO_X abatement. Curr Opin Chem Eng 2016;13:133–41. https://doi.org/10.1016/j.coche.2016.09.004.

[9] Kang L, Pan W, Zhang J, Wang W, Tang C. A review on ammonia blends combustion for industrial applications. Fuel 2023;332:126150. https://doi.org/10.1016/j.fuel.2022.126150.

[10] Kurien C, Mittal M. Review on the production and utilization of green ammonia as an alternate fuel in dual-fuel compression ignition engines. Energ Conver Manage 2022;251:114990. https://doi.org/10.1016/j.enconman.2021.114990.

[11] Cai T, Zhao D, Gutmark E. Overview of fundamental kinetic mechanisms and emission mitigation in ammonia combustion. Chem Eng J 2023;458:141391. https://doi.org/10.1016/j.cej.2023.141391.

[12] Chen X, Liu Q, Zhao W, Li R, Zhang Q, Mou Z. Experimental and chemical kinetic study on the flame propagation characteristics of ammonia/hydrogen/air mixtures. Fuel 2023;334:126509. https://doi.org/10.1016/j.fuel.2022.126509.

[13] Zhao H, Zhao D, Becker S, Zhang Y. NO emission and enhanced thermal performances studies on counter-flow double-channel hydrogen/ammonia-fuelled microcombustors with oval-shaped internal threads. Fuel 2023;341:127665. https://doi.org/10.1016/j.fuel.2023.127665.

[14] Ni S, Zhao D, Wu W, Guan Y. NO_X emission reduction reaction of ammonia-hydrogen with self-sustained pulsating oscillations. Therm Sci Eng Progr 2020;19:100615. https://doi.org/10.1016/j.tsep.2020.100615.

[15] Yang W, Ranga Dinesh KKJ, Luo KH, Thévenin D. Direct numerical simulations of auto-igniting mixing layers in ammonia and ammonia-hydrogen combustion under engine-relevant conditions. Int J Hydrogen Energy 2022;47:38055–74. https://doi.org/10.1016/j.ijhydene.2022.08.290.

[16] Chen Z, Jiang Y. Numerical investigation of the effects of H_2/CO/syngas additions on laminar premixed combustion characteristics of NH_3/air flame. Int J Hydrogen Energy 2021;46:12016–30. https://doi.org/10.1016/j.ijhydene.2021.01.054.

[17] Cai T, Zhao D. Enhancing and assessing ammonia-air combustion performance by blending with dimethyl ether. Renew Sustain Energy Rev 2022;156:112003. https://doi.org/10.1016/j.rser.2021.112003.

[18] Issayev G, Giri BR, Elbaz AM, Shrestha KP, Mauss F, Roberts WL, et al. Ignition delay time and laminar flame speed measurements of ammonia blended with dimethyl ether: A promising low carbon fuel blend. Renew Energy 2022;181:1353–70. https://doi.org/10.1016/j.renene.2021.09.117.

[19] Zhang Q, Guo L, Cai X, Shan S, Li K, Zhao J, et al. Chemical effect of CH_4 on NH_3 combustion in an O_2/N_2 environment via ReaxFF. Energy Fuel 2021;35:10918–28. https://doi.org/10.1021/acs.energyfuels.1c01016.

[20] Chiong M-C, Chong CT, Ng J-H, Mashruk S, Chong WWF, Samiran NA, et al. Advancements of combustion technologies in the ammonia-fuelled engines. Energ Conver Manage 2021;244:114460. https://doi.org/10.1016/j.enconman.2021.114460.

[21] Nadimi E, Przybyła G, Lewandowski MT, Adamczyk W. Effects of ammonia on combustion, emissions, and performance of the ammonia/diesel dual-fuel compression ignition engine. J Energy Inst 2023;107:101158. https://doi.org/10.1016/j.joei.2022.101158.

[22] Andreae MO, Ramanathan V. Climate’s dark forcings. Science 2013;340:280–1. https://doi.org/10.1126/science.1235731.

[23] Cheng X, Li Y, Xu Y, Liu Y, Wang B. Study of effects of ammonia addition on soot formation characteristics in n-heptane co-flow laminar diffusion flames. Combust Flame 2022;235:111683. https://doi.org/10.1016/j.combustflame.2021.111683.

[24] Zhang K, Xu Y, Li Y, Liu Y, Wang B, Wang H, et al. Effects of ammonia on morphological characteristics and nanostructure of soot in the combustion of diesel surrogate fuels. J Hazard Mater 2023;445:130645. https://doi.org/10.1016/j.jhazmat.2022.130645.

[25] Zhu J, Liu X, Xu Y, Xu J, Wang H, Zhang K, et al. Probing into volatile combustion flame and particulate formation behavior during the coal and ammonia co-firing process. Energy Fuel 2022;36:9347–56. https://doi.org/10.1021/acs.energyfuels.2c01450.

[26] Cheng JJ, Timilsina GR. Status and barriers of advanced biofuel technologies: A review. Renew Energy 2011;36:3541–9. https://doi.org/10.1016/j.renene.2011.04.031.

[27] Virgínio e Silva JO, Almeida MF, da Conceição Alvim-Ferraz M, Dias JM. Integrated production of biodiesel and bioethanol from sweet potato. Renew Energy 2018;124:114–20. https://doi.org/10.1016/j.renene.2017.07.052.

[28] Kumar V, Nanda M, Joshi HC, Singh A, Sharma S, Verma M. Production of biodiesel and bioethanol using algal biomass harvested from fresh water river. Renew Energy 2018;116:606–12. https://doi.org/10.1016/j.renene.2017.10.016.
[29] Hosseinzadeh-Bandbafha H, Rafiee S, Mohammadi P, Ghobadian B, Lam SS, Tabatabaei M, et al. Exergetic, economic, and environmental life cycle assessment analyses of a heavy-duty tractor diesel engine fueled with diesel–biodiesel-bioethanol blends. Energ Conver Manage 2021;241:114300. https://doi.org/10.1016/j.enconman.2021.114300.
[30] Kalligeros S, Zannikos F, Stournas S, Lois E, Anastopoulos G, Teas C, et al. An investigation of using biodiesel/marine diesel blends on the performance of a stationary diesel engine. Biomass Bioenergy 2003;24:141–9. https://doi.org/10.1016/S0961-9534(02)00092-2.
[31] Benjumea P, Agudelo J, Agudelo A. Basic properties of palm oil biodiesel–diesel blends. Fuel 2008;87:2069–75. https://doi.org/10.1016/j.fuel.2007.11.004.
[32] Sivasubramanian R, Sajin JB, Omanakuttan PG. Effect of ammonia to reduce emission from biodiesel fuelled diesel engine. Int J Ambient Energy 2022;43:661–5. https://doi.org/10.1080/01430750.2019.1663367.
[33] Nadimi E, Przybyła G, Emberson D, Løvås T, Ziółkowski Ł, Adamczyk W. Effects of using ammonia as a primary fuel on engine performance and emissions in an ammonia/biodiesel dual-fuel CI engine. Int J Energy Res 2022;46:15347–61. https://doi.org/10.1002/er.8235.
[34] Ronan P, Pierre B, Christine M-R, Guillaume D, Fabien H. Laminar flame speed of ethanol/ammonia blends–An experimental and kinetic study. Fuel Commun 2022;10:100052. https://doi.org/10.1016/j.jfueco.2022.100052.
[35] Cardoso JS, Silva V, Chavando JAM, Eusébio D, Hall MJ. Numerical modelling of the coal phase-out through ammonia and biomass co-firing in a pilot-scale fluidized bed reactor. Fuel Commun 2022;10:100055. https://doi.org/10.1016/j.jfueco.2022.100055.
[36] Li X, Zheng M, Ren C, Guo L. ReaxFF molecular dynamics simulations of thermal reactivity of various fuels in pyrolysis and combustion. Energy Fuel 2021;35:11707–39. https://doi.org/10.1021/acs.energyfuels.1c01266.
[37] Wang J, Jiang XZ, Luo KH. Exploring reaction mechanism for ammonia/methane combustion via reactive molecular dynamics simulations. Fuel 2023;331:125806. https://doi.org/10.1016/j.fuel.2022.125806.
[38] Zhang P, Zhang K, Cheng X, Liu Y, Wu H. Analysis of inhibitory mechanisms of ammonia addition on soot formation: A combined ReaxFF MD simulations and experimental study. Energy Fuel 2022;36:12350–64. https://doi.org/10.1021/acs.energyfuels.2c02206.
[39] Gaïl S, Sarathy SM, Thomson MJ, Diévart P, Dagaut P. Experimental and chemical kinetic modeling study of small methyl esters oxidation: Methyl (E)-2-butenoate and methyl butanoate. Combust Flame 2008;155:635–50. https://doi.org/10.1016/j.combustflame.2008.04.007.
[40] Gaïl S, Thomson MJ, Sarathy SM, Syed SA, Dagaut P, Diévart P, et al. A wide-ranging kinetic modeling study of methyl butanoate combustion. Proceedings of the Combustion Institute 2007;31:305–11. 10.1016/j.proci.2006.08.051.
[41] Wang Y, Mao Q, Wang Z, Luo KH, Zhou L, Wei H. A ReaxFF molecular dynamics study of polycyclic aromatic hydrocarbon oxidation assisted by nitrogen oxides. Combust Flame 2023;248:112571. https://doi.org/10.1016/j.combustflame.2022.112571.
[42] Plimpton S. Fast parallel algorithms for short-range molecular dynamics. J Comput Phys 1995;117:1–19. https://doi.org/10.1006/jcph.1995.1039.
[43] Kowalik M, Ashraf C, Damirchi B, Akbarian D, Rajabpour S, van Duin ACT. Atomistic scale analysis of the carbonization process for C/H/O/N-based polymers with the ReaxFF reactive force field. J Phys Chem B 2019;123:5357–67. https://doi.org/10.1021/acs.jpcb.9b04298.
[44] van Duin ACT, Dasgupta S, Lorant F, Goddard WA. ReaxFF: A reactive force field for hydrocarbons. Chem A Eur J 2001;105:9396–409. https://doi.org/10.1021/jp004368u.
[45] Mayo SL, Olafson BD, Goddard WA. DREIDING: a generic force field for molecular simulations. J Phys Chem 1990;94:8897–909. https://doi.org/10.1021/j100389a010.
[46] Stukowski A. Visualization and analysis of atomistic simulation data with OVITO-the Open Visualization Tool. Model Simul Mater Sci Eng 2010;18:015012. https://doi.org/10.1088/0965-0393/18/1/015012.
[47] Zeng J, Cao L, Chin C-H, Ren H, Zhang JZH, Zhu T. ReacNetGenerator: an automatic reaction network generator for reactive molecular dynamics simulations. PCCP 2020;22:683–91. https://doi.org/10.1039/C9CP05091D.
[48] Johansson KO, Head-Gordon MP, Schrader PE, Wilson KR, Michelsen HA. Resonance-stabilized hydrocarbon-radical chain reactions may explain soot inception and growth. Science 2018;361:997–1000. https://doi.org/10.1126/science.aat3417.
[49] Pope CJ, Miller JA. Exploring old and new benzene formation pathways in low-pressure premixed flames of aliphatic fuels. Proceedings of the Combustion Institute 2000;28:1519–27. 10.1016/S0082-0784(00)80549-4.
[50] Frenklach M. Reaction mechanism of soot formation in flames. PCCP 2002;4:2028–37. https://doi.org/10.1039/b110045a.
[51] Wang Q-D, Wang J-B, Li J-Q, Tan N-X, Li X-Y. Reactive molecular dynamics simulation and chemical kinetic modeling of pyrolysis and combustion of n-dodecane. Combust Flame 2011;158:217–26. https://doi.org/10.1016/j.combustflame.2010.08.010.
[52] Ashraf C, Shabnam S, Jain A, Xuan Y, van Duin ACT. Pyrolysis of binary fuel mixtures at supercritical conditions: A ReaxFF molecular dynamics study. Fuel 2019;235:194–207. https://doi.org/10.1016/j.fuel.2018.07.077.
[53] Zhang Y, Wang X, Li Q, Yang R, Li C. A ReaxFF molecular dynamics study of the pyrolysis mechanism of oleic-type triglycerides. Energy Fuel 2015;29:5056–68. https://doi.org/10.1021/acs.energyfuels.5b00720.
[54] Campbell MF, Davidson DF, Hanson RK. Ignition delay times of very-low-vapor-pressure biodiesel surrogates behind reflected shock waves. Fuel 2014;126:271–81. https://doi.org/10.1016/j.fuel.2014.02.050.
[55] Zhao J, Lin Y, Huang K, Gu M, Lu K, Chen P, et al. Study on soot evolution under different hydrogen addition conditions at high temperature by ReaxFF molecular dynamics. Fuel 2020;262:116677. https://doi.org/10.1016/j.fuel.2019.116677.
[56] Zhang K, Xu Y, Liu Y, Wang H, Liu Y, Cheng X. Effects of ammonia addition on soot formation in ethylene laminar diffusion flames. Part 2. Further insights into soot inception, growth and oxidation. Fuel 2023;331:125623. https://doi.org/10.1016/j.fuel.2022.125623.